

CIRCULARLY POLARIZED ARRAYS OF CAVITY BACKED SLOT ANTENNAS FOR X-BAND SATELLITE COMMUNICATIONS

E. M. A. Eldesouki and K. F. A. Hussein

Microwave Engineering Department
Electronics Research Institute
Cairo, Egypt

A. A. El-Nadi

Electronics and Electrical Communications Department
Faculty of Engineering
Cairo University
Egypt

Abstract—Circularly-polarized arrays of cavity backed slot (CBS) antennas are proposed for X-band satellite-earth communications. Two configurations of such circularly polarized arrays are investigated: cross-shaped and square-shaped arrays. Both configurations can produce right-hand circular polarization (RHCP) as well as left-hand circular polarization (LHCP) by proper setting of excitation phase for each element in the array. The finite-difference time-domain (FDTD) method is used to analyze the characteristics of the proposed arrays including the input impedance, S -parameters, radiation pattern, gain and axial ratio. The results show that the proposed array configurations seem very promising and useful for geostationary satellite applications.

1. INTRODUCTION

For the applications of geostationary earth orbit (GEO) satellites and radar systems of high-speed vehicles or aircraft, low profile and circularly polarized antennas are the most eligible choice. Most GEO satellites use circular polarization for their RF systems which allow them to transmit and receive multiple or arbitrary signals without requiring the alignment of the electric field vector at the receiving and

transmitting locations. A CBS antenna has simple structure and small mutual effects between elements when arranged in a planar array.

CBS scatterers and antennas are famous for their internal resonance [14–23] and have been analyzed using various methods such as the integral equation solution by the method of moments (MOM) [1, 2], finite element method (FEM) [3] and finite-difference time-domain (FDTD) method [4–6]. In this paper, the analysis of the CBS antenna is performed using FDTD method [11, 12] because of its ability to model complex structures especially when they are made of planar surfaces or piecewise rectangular blocks. Moreover, the FDTD can easily model thin wires, which are often used as excitation for CBS antennas. In addition, the FDTD method has the advantage of being able to provide the frequency response of the CBS antenna from a single run of the FDTD algorithm by applying the proper selection of a time-domain-pulse excitation and then calculating the discrete Fourier Transform (DFT) for the quantities of interest.

So far the published results have shown that a CBS antenna excited in the TE_{101} mode is linearly polarized. Different configurations of CBS antenna have been examined for producing circularly polarized radiation, such as single square loop slot, two element square loop slot and two-arm spiral slot antenna [7]. In this work, cross-shaped and square-shaped arrays, are proposed to produce circular polarization for X-band satellite communications with high gain, and high front-to-back ratio (FBR).

This paper is divided into four main sections. The first one describes the structure of the CBS antenna, cross-shaped and square-shaped arrays. The second part describes the method used to calculate the input impedance and to study the radiation characteristics of the proposed arrays. The third section presents the results for the CBS antenna and the proposed arrays.

2. ANTENNA STRUCTURE AND DESIGN

Figure 1 illustrates the structure of the CBS antenna. The dimensions of the cavity ($a \times b \times c$) should be set so that TE_{10n} modes; $n = 1, 2, 3 \dots$ can be excited in the cavity. The CBS antenna is constructed as an open ended rectangular waveguide which is mounted at the center of a rectangular conducting plate with an aperture that coincides with the open end of the waveguide. The dimensions of the conducting plate, $W_x \times W_y$, do not have a profound effect on the value of the input impedance as long as they are large enough [6]. The CBS antenna is fed by a monopole located inside the cavity at $(a/2, b, c)$ with its base attached to one of the waveguide walls as shown in Fig. 1. The

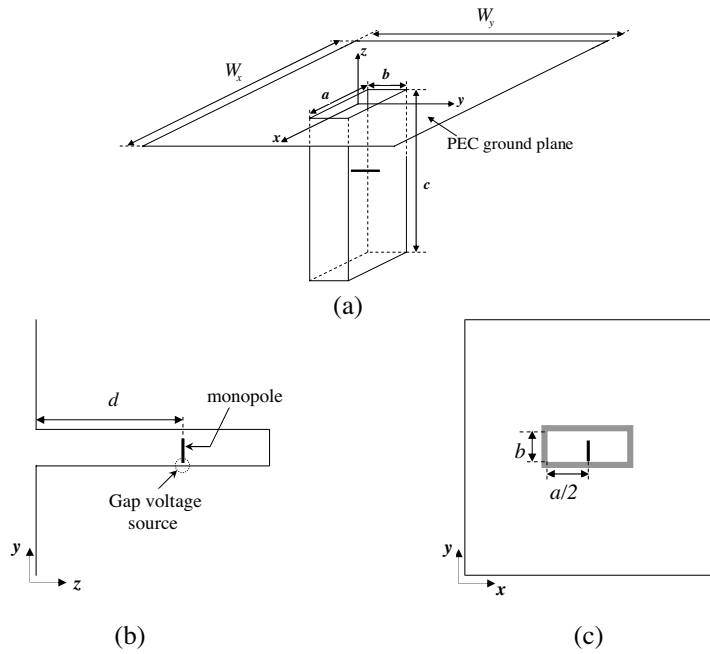


Figure 1. Geometry of a rectangular CBS antenna fed with a probe (monopole). (a) 3-D view. (b) Side view. (c) Top view.

excitation is carried out by delta-gap voltage source attached to the base of the monopole. It is worth noting that this monopole replaces the actual excitation which is usually a probe made as an extension of the inner conductor of a coaxial feeder.

Figure 2 shows cross-shaped and square-shaped arrays designed to produce circular polarization. Both arrays are composed of 4 identical CBS elements, with d_s spacing between the array elements. The arrays are mounted on a rectangular conducting plate of dimensions $W_x \times W_y$. Each element in the array is excited by a monopole which is oriented in either x - or y -direction. Each monopole is excited by a gap voltage generator at its base with respect to waveguide wall. The excitations of the 4-monopole elements are carried out in phase quadrature to achieve circular polarization.

3. CBS ANTENNA ANALYSIS USING FDTD METHOD

The FDTD method is adopted to analyze cross-shaped and square-shaped CBS antenna arrays. Yee's algorithm is used with uniaxial

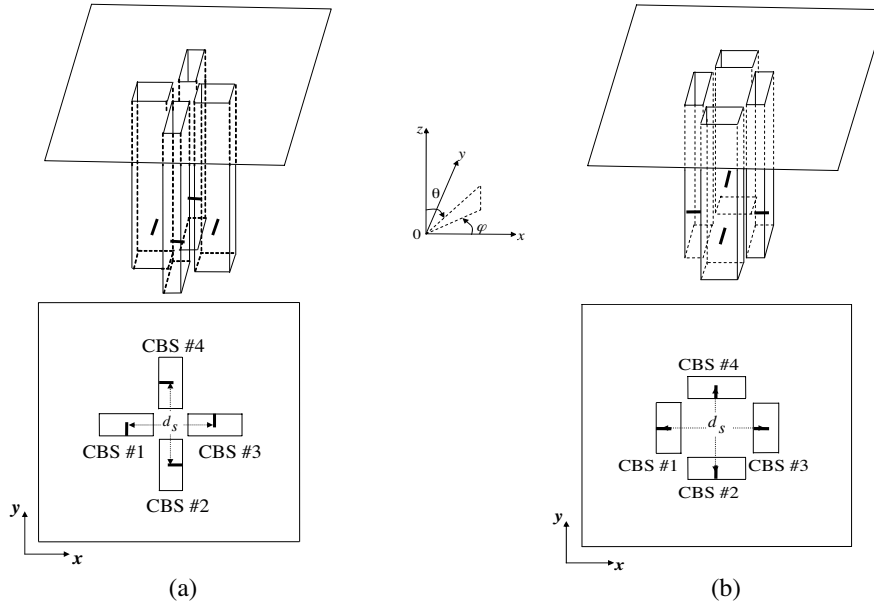


Figure 2. Two array configurations proposed to produce circular polarization. (a) Cross-shaped array. (b) Square-shaped array.

perfectly matched layer (UPML) absorbing boundary conditions. Reasonable spacing is left between the antenna or array structure and the absorbing boundary in each direction of the axis coordinates. The excitation is modeled by a delta-gap-voltage source with internal resistance of $50\ \Omega$ to reduce the number of time steps required for FDTD calculations for such type of resonant antenna. The power loss results only from radiation since all metallic surfaces are assumed to be perfect conductors and region inside the cavity is assumed to be a vacuum.

The input impedance of the antenna ($Z_{in} = R_{in} + jX_{in}$) is obtained by calculating the current and voltage at the base of the monopole due to a time-domain Gaussian-pulsed voltage source. Then, the time domain quantities $v(t)$ and $i(t)$ are transformed to frequency domain quantities $V(\omega)$ and $I(\omega)$ by applying a discrete Fourier transform (DFT) procedure.

The far-field patterns can be obtained by using near-to-far field transformation. A virtual surface, S' , is assumed to enclose the radiating structure and to lie entirely in the free space region (solution domain of the FDTD) without intercepting or touching the absorbing

layers [10]. The time domain electric current $\mathbf{J}_s = \hat{\mathbf{n}} \times \mathbf{H}(t, \mathbf{r}')$, and the magnetic current $\mathbf{M}_s = -\hat{\mathbf{n}} \times \mathbf{E}(t, \mathbf{r}')$ on S' , where \mathbf{r}' is the position vector of the source point on S' at which \mathbf{E} and \mathbf{H} are evaluated on the closed surface and $\hat{\mathbf{n}}$ is the outward unit vector normal to S' . The θ and φ components of the radiation field at a far point (r, θ, φ) are given as:

$$E_\theta = \frac{-jk_e^{-jk_o r}}{4\pi r} (L + \eta_o N) \quad (1)$$

$$E_\phi = \frac{jk_e^{-jk_o r}}{4\pi r} (L + \eta_o N) \quad (2)$$

with

$$N = \iint_S J_s e^{-jk_o r \cos \psi} dS' \quad (3)$$

$$L = \iint_S M_s e^{-jk_o r \cos \psi} dS' \quad (4)$$

where k_o is the wave number in the free space, η_o is the intrinsic impedance and r is the position of the observation point on the virtual surface S' .

After the radiation field $E_\theta \hat{\mathbf{a}}_\theta + E_\phi \hat{\mathbf{a}}_\phi$ is decomposed into RHCP wave component: $E_R (\hat{\mathbf{a}}_\theta - j\hat{\mathbf{a}}_\phi) / \sqrt{2}$ and a LHCP wave component: $E_L (\hat{\mathbf{a}}_\theta + j\hat{\mathbf{a}}_\phi) / \sqrt{2}$, the circular components can be expressed as:

$$E_R = \frac{1}{\sqrt{2}} (E_\theta + jE_\phi) \quad \text{and} \quad E_L = \frac{1}{\sqrt{2}} (E_\theta - jE_\phi) \quad (5)$$

The E_θ , E_ϕ , E_R , and E_L have the following relationship:

$$|E_\theta|^2 + |E_\phi|^2 = |E_R|^2 + |E_L|^2 \quad (6)$$

The absolute gain is evaluated using the following equation:

$$G = 4\pi \frac{\text{radiation intensity}}{\text{input power}} = 4\pi \frac{U(\theta, \phi)}{P_{in}} \quad (7)$$

where:

$$U(\theta, \phi) = \frac{0.5r^2 \left(|E_\theta^2| + |E_\phi^2| \right)}{120\pi} \quad (8)$$

$$P_{in} = 0.5|V(\omega)| |I(\omega)| \cos(\psi) \quad (9)$$

The gain of the antenna is given by:

$$G = \frac{r^2 (|E_\theta|^2 + |E_\phi|^2)}{30|V(\omega)||I(\omega)|\cos(\psi)} \quad (10)$$

where, $V(\omega)$ and $I(\omega)$ are the values of the voltage and current at the input terminal respectively and ψ is the phase difference between $V(\omega)$ and $I(\omega)$.

The antenna gain for the RHCP and LHCP at a far-field point is evaluated as G_R and G_L , respectively, which can be expressed as:

$$G_R = |E_R|^2 r^2 / 30P_{in} \quad (11)$$

$$G_L = |E_L|^2 r^2 / 30P_{in} \quad (12)$$

The axial ratio can be expressed as:

$$AR = \frac{|E_R| + |E_L|}{|E_R| - |E_L|} \quad (13)$$

4. RESULTS AND DISCUSSIONS

An open-ended rectangular waveguide operating as CBS antenna is analyzed using FDTD method. A computer program for the implementation of the FDTD algorithm is developed by the authors using C++ language. The FDTD lattice dimensions are $154.5 \times 154.5 \times 133.5$ mm comprised of cubic Yee cells each of 1.5 mm side length (corresponds to $0.034\lambda_o$ at a frequency of 6.8 GHz), with 12 mm thickness of the absorbing boundary layer. There are 15 mm spacing between the radiating structure and the absorbing boundary in each direction of the coordinate system axes. The excitation is modeled by a delta-gap voltage source with internal source resistance of 50Ω . The function of such a resistance is to reduce the time required for the FDTD algorithm to reach the steady state by rapidly damping the oscillations resulting from the cavity resonance. The radius of the monopole is 0.000635 mm and is represented using thin wire model [9]. Field components are updated every 2.88675 ps; this time step satisfies the condition for numerical stability stated by Courant [8, 13].

To verify the validity of the numerical results for the CBS antenna obtained by the applied FDTD algorithm, they are compared with those obtained in [6] for the same antenna. The results obtained for the input impedance against the frequency are compared to those presented in [6]. The dependence of the gain of a single CBS antenna on the location of the exciting monopole is investigated at different

frequencies. The radiation patterns of a single CBS antenna are presented over a wide frequency range. The characteristics of the cross-shaped and square-shaped CBS antenna arrays are investigated over the operating frequency band. The frequency responses of the gain and axial ratio are presented and discussed. The radiation patterns for the RHCP and LHCP components are also investigated.

4.1. Characteristics of a Single CBS Antenna

The CBS antenna is constructed up of a standard open-ended rectangular waveguide (WR-90) with internal dimensions of $22.86 \times 10.16 \times 77.55$ mm, mounted on a 100×100 mm ground plane. The excitations applied at the input port to investigate the characteristics of the CBS antenna are a ramped-amplitude sinusoidal source and a differentiated Gaussian pulse. The excitation signal is applied at the base of a monopole of 6.985 mm length. The time waveforms and frequency spectra of the applied signals are shown in Fig. 3. The FDTD algorithm runs until steady state is reached everywhere.

4.1.1. Input Impedance of a CBS Antenna

Figure 4 shows the input impedance of the CBS antenna which is computed using a differentiated Gaussian pulse with an internal source resistance of 50Ω to reduce the computational time required for the monopole current pulse to vanish. The frequency response of the antenna input impedance is compared with that obtained in [6]. The comparison shows good agreement which ensures the validity of the applied FDTD algorithm and the C++ program developed by the authors.

Good results for S_{11} and VSWR are obtained when the exciting monopole is placed at $d = 67.5$ mm. The frequency response of the input impedance and $|S_{11}|$ are shown in Figs. 5 and 6, respectively. The VSWR for this antenna is presented in Fig. 7, assuming a source impedance of 75Ω . Table 1 displays the results of $|S_{11}|$, VSWR, and the corresponding bandwidth within which the VSWR is maintained below 2.

4.1.2. Field Distribution inside the Rectangular Waveguide Cavity of the CBS Antenna

Several modes of electromagnetic waves can be excited in the cavity. The physical dimensions of the cavity determine the cut off frequency of each mode. It is well known that the internal field in a cavity is enhanced at the frequencies corresponding to the cavity resonances. At

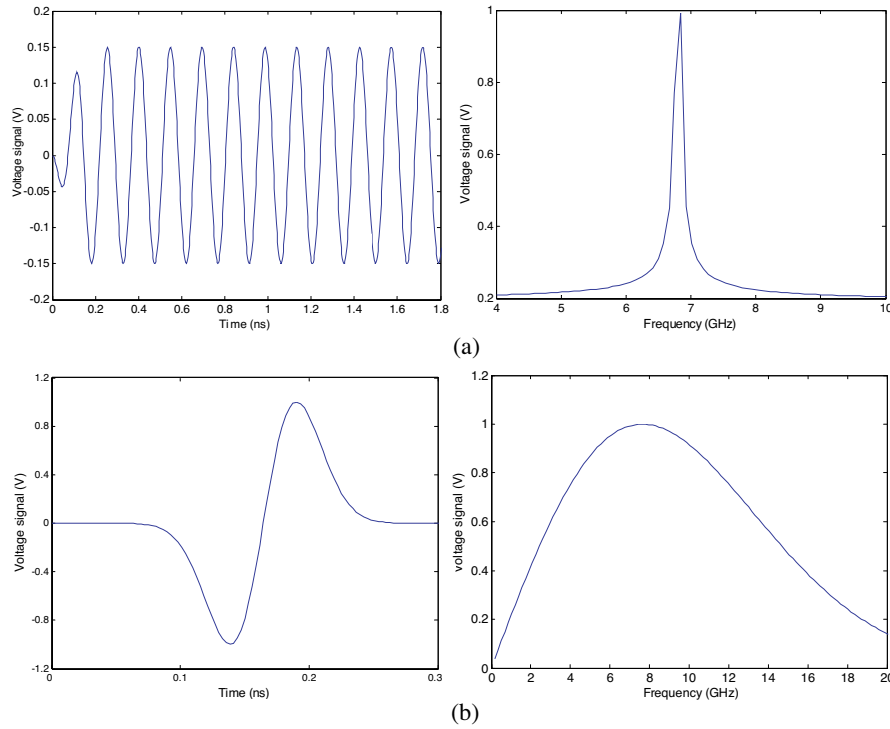


Figure 3. Time waveforms and Frequency spectra of (a) ramped-sinusoidal source, (b) differentiated Gaussian pulse.

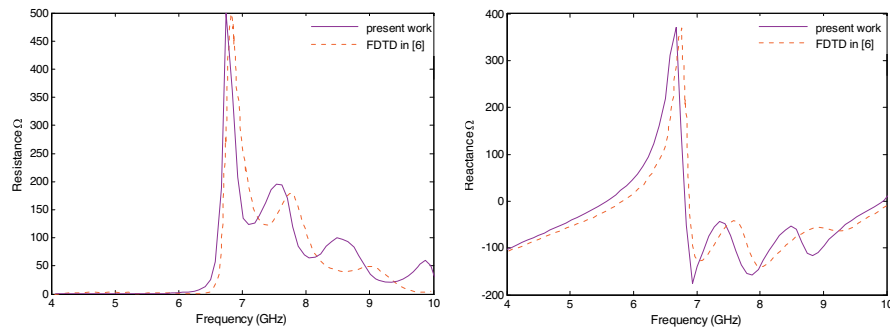


Figure 4. Frequency response of the input impedance of a CBS antenna, $d = 58.5$ mm.

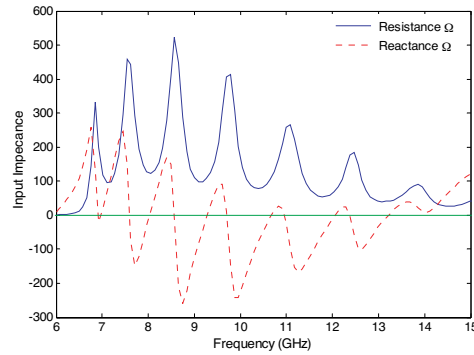


Figure 5. Frequency response of the input impedance of a CBS antenna, $d = 67.5$ mm.

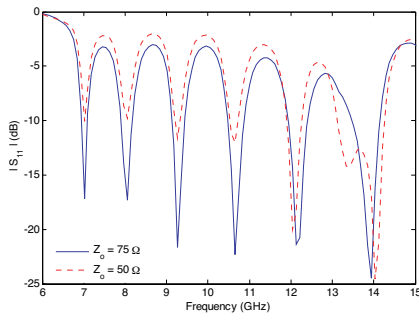


Figure 6. Frequency response of $|S_{11}|$ at $d = 67.5$ mm.

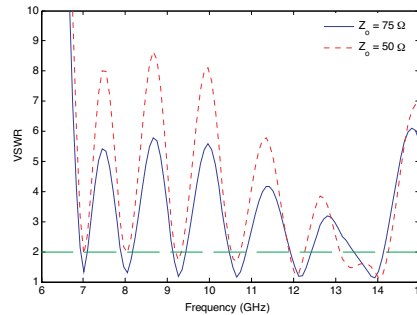


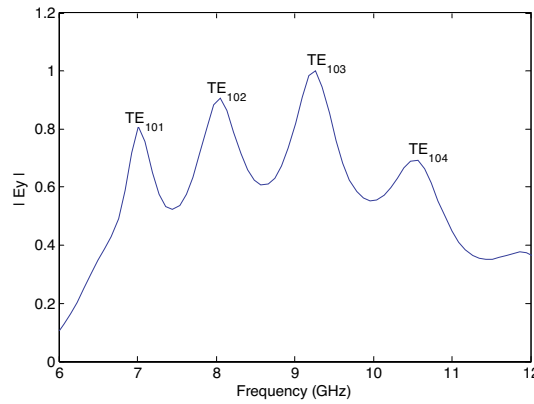
Figure 7. Frequency response of the VSWR at $d = 67.5$ mm.

such resonant frequencies, the internal field distributions exhibit the corresponding modal field configurations. This is investigated with graphical presentation in the following discussion. Fig. 8 shows the frequency response of the electric field (E_y component) normalized to its maximum value at 9.3 GHz. This curve is obtained by calculating the DFT of E_y at $x = 15.93$ mm, $y = 3.75$ mm and $z = 61.5$ mm due to a differentiated Gaussian pulse as that shown in Fig. 3(b). It can be shown from Fig. 8 that, there are four peaks obtained at 7.02, 8.1, 9.3 and 10.57 GHz which are corresponding to TE_{101} , TE_{102} , TE_{103} and TE_{104} modes, respectively.

Time-domain snapshots (at $t = 5.77$ ns) for the electric field distribution (E_y -component) at the internal resonances of the waveguide cavity when excited by a sinusoidal voltage source with the corresponding frequency are shown in Fig. 9. In the x - y plane

Table 1. The result of $|S_{11}|$ and bandwidth assuming $Z_o = 75 \Omega$.

f (GHz)	S_{11} (dB)	VSWR	Bandwidth (GHz)
7.06	-17.4	1.33	0.16 (6.9–7.1)
8.1	-17.45	1.28	0.28 (7.9–8.2)
9.3	-21.51	1.18	0.31 (9.2–9.4)
10.66	-23	1.16	0.4 (10.5–10.7)
12.18	-21.17	1.18	0.46 (11.9–12.4)

**Figure 8.** Frequency response of the normalized electric field.

the data shows a cosine distribution along the x -axis and a uniform distribution along the y -axis. This comes in agreement with the known field distribution for E_y of the TE_{10n} modes. In the x - z plane, there are standing wave patterns along the length of the waveguide section. The number of cycles observed in the internal field patterns determines the order of the corresponding resonant mode.

4.1.3. Far Field Radiation Patterns for a Single CBS Antenna

The radiation patterns for the CBS antenna are obtained at TE_{101} and TE_{102} resonance modes. Fig. 10 shows the elevation gain patterns (with respect to θ) in the E -plane ($\varphi = 0^\circ$) and H -plane ($\varphi = 90^\circ$) and the azimuth gain patterns (with respect to φ on the cone $\theta = 15^\circ$), respectively. Good omnidirectional radiation patterns in the azimuth plane are observed. In the elevation plane, the beams are symmetric

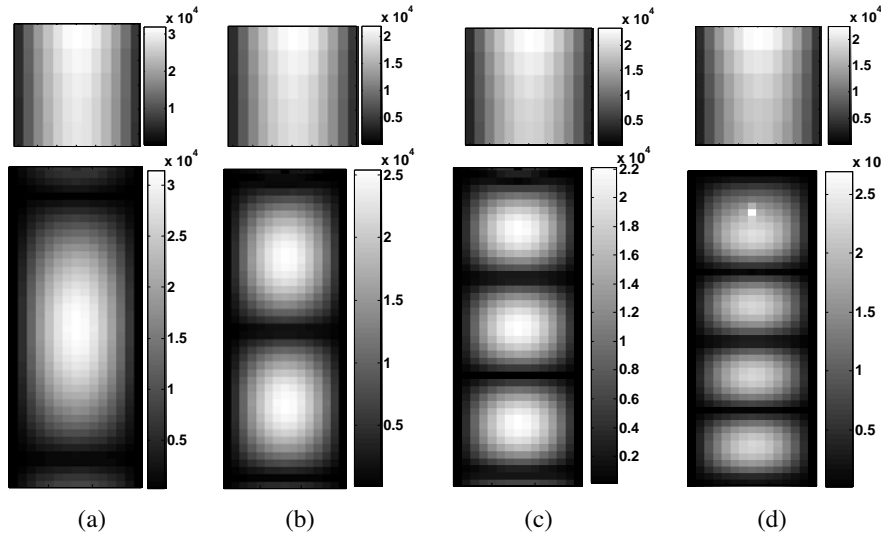


Figure 9. Time-domain snap-shots for the electric field distribution (E_y -component) at $t = 5.77$ ns in the planes x - y and x - z plane at the resonances (a) TE_{101} (7.01 GHz), (b) TE_{102} (8 GHz), (c) TE_{103} (9.3 GHz) and (d) TE_{104} (10.57 GHz).

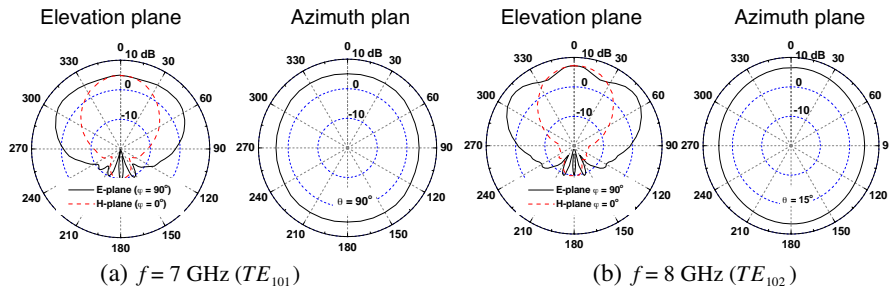


Figure 10. E -plane and H -plane gain patterns for a CBS antenna at the cavity resonances.

and hve HPBW of 150° for the E -plane, and 70° for the H -plane. The antenna gain at 7 and 8 GHz are 4.8 and 6.7 dBi, respectively.

4.2. Circularly Polarized Arrays

A single CBS antenna generally radiates linear polarization. In order to obtain circular polarization; two sets of linearly polarized CBS

antennas are orthogonally arranged in cross-shaped and square-shaped configurations as shown in Fig. 2, with an array distance $d_s = 36$ mm ($0.8164\lambda_{6.84}$) in both x and y directions. The other array parameters are defined in Section 4.1. The array elements are simultaneously excited with equal amplitude and $\pm 90^\circ$ progressive phase difference where the \pm sign determining the direction of phase circulation which, in turn, determines the sense of polarization according to the specific array configuration.

4.2.1. Scattering Matrix of Cross-Shaped and Square-Shaped Arrays

Each of the array configurations has four ports. The elements of the scattering matrices of the cross-shaped and square-shaped arrays are plotted against the frequency as shown in Fig. 6 and Fig. 11, respectively. Due to circuit symmetry, the diagonal elements of the scattering matrix are equal ($S_{11} = S_{22} = S_{33} = S_{44}$) and the matrix itself is symmetric ($S_{ij} = S_{ji}$, $i = 1, 2, 3, 4$, $j = 1, 2, 3, 4$).

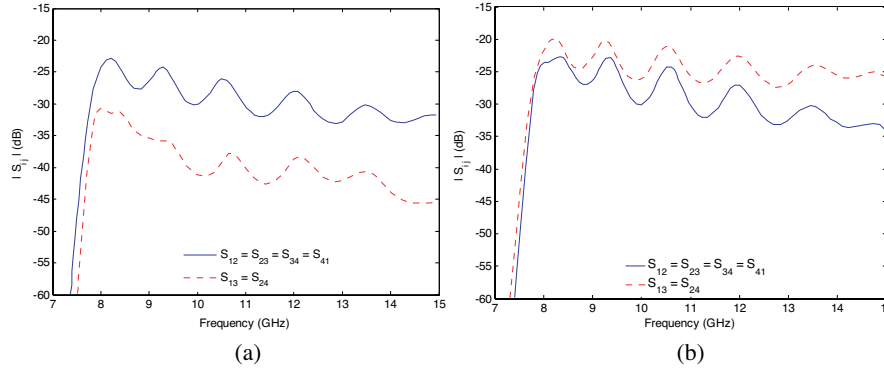


Figure 11. Frequency response of the coupling coefficients S_{ij} for both array configurations: (a) Cross-shaped array and (b) Square array.

The relative positions of each of the elements #1, #2, #3 and #4 with respect to each of the elements #2, #3, #4 and #1, respectively, are the same in both array configurations. This causes the corresponding mutual scattering parameters S_{12} , S_{23} , S_{34} and S_{41} to be almost the same for both array configurations. This is clear when comparing the solid-line curves in Figs. 11(a) and 11(b). This is not the same for the mutual scattering parameters S_{13} and S_{24} for each array since the relative positions of the elements #1, #2 relative to the elements #3, #4, respectively, are not the same in the two arrays. The square-shaped array configuration results in stronger coupling between

the facing elements, which becomes clear by comparing the dashed-line curves in Figs. 11(a) and 11(b).

4.2.2. Radiation Characteristics of the Cross-Shaped Array

A cross-shaped array as shown in Fig. 2(a) is excited with equal amplitudes and $+90^\circ$ progressive phase shift to obtain RHCP. Fig. 12 shows the RHCP and LHCP radiation patterns in the elevation plane $\varphi = 90^\circ$ and the cone $\theta = 15^\circ$ at different frequencies. The radiation pattern is perfectly omnidirectional in the azimuth plane and on the cones of constant θ .

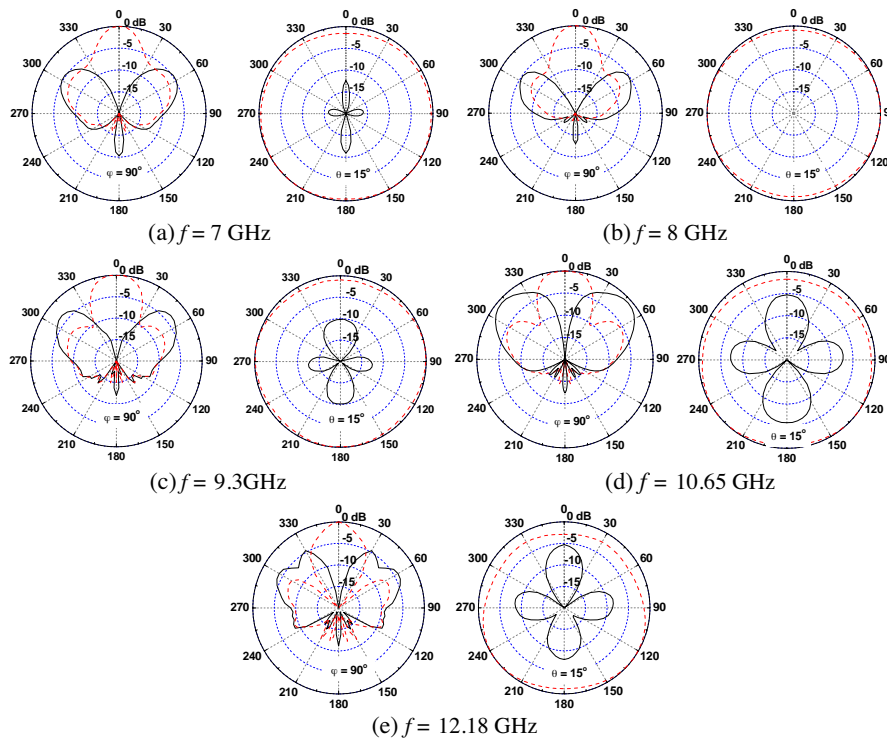


Figure 12. Radiation patterns for the circularly polarized components obtained for cross-shaped array (solid line represents LHCP, dashed line represents RHCP).

Figure 13 shows the axial ratio of the cross-shaped array at 7 GHz in the elevation plane $\varphi = 90^\circ$ and on the cone $\theta = 15^\circ$. From the radiation patterns in the elevation plane appearing in Figures 12 and 13, it is seen that the cross-shaped array produces perfect circular

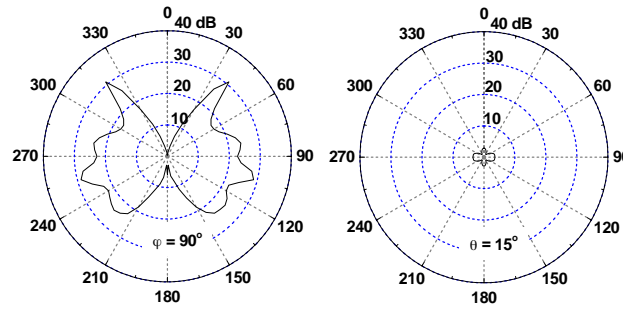


Figure 13. Axial ratio patterns for the cross-shaped array at $f = 7$ GHz.

polarization in the forward directions determined by ($|\theta| < 28^\circ$) especially over narrow frequency bands around the cavity resonances.

The properties of these patterns are summarized in Table 2. Good RHCP radiation characteristics are obtained up to 9 GHz. The radiation pattern starts to deteriorate at 11 GHz. For the frequencies less than 11 GHz, the antenna has a beam width that ranges from 32° to 48° . The cross-shaped array has a maximum gain of 13 dBi and maximum front to back ratio of 30 dB.

Table 2. Far field radiation properties for cross-shaped array.

f (GHz)	3 dB BW	FBR (dB)	Gain (dBi)
7	36°	22.77	11.8
8	32°	30	12.7
9.3	40°	15	11.9
10.65	48°	26.4	7.37
12.18	30.8°	27.5	11.2

Figure 14 shows the array gain for the RHCP component as a function of the parameter d in the direction $\theta = 0^\circ$ and $\varphi = 90^\circ$ at $f = 6.84$ GHz compared with the gain of a single CBS antenna. From this figure, we can see that the high gain (of about 13 dBi) is obtained at $d = 21.5$ mm and $d = 67.5$ mm, the values of d which are approximately corresponding to 0.5λ and 1.5λ , respectively. The variation in the axial ratio against the distance d is presented in Fig. 15. It should be noted that good values of the axial ratio (close to 0 dB) are obtained at the same values of d .

Figure 16 shows the frequency response of the RHCP gain in the direction $\theta = 0^\circ$ and $\varphi = 90^\circ$. From this figure, it can be observed that the RHCP gain of the cross-shaped array is increased to about 7 dB above the gain of the single element over the frequency band (6.8–10.6 GHz), and to about 6 dBi over the frequency band (11.2–13 GHz). From the frequency response of the axial ratio presented in Fig. 17, it is seen that good circular polarization is obtained at the frequency corresponding the resonant modes of the cavity.

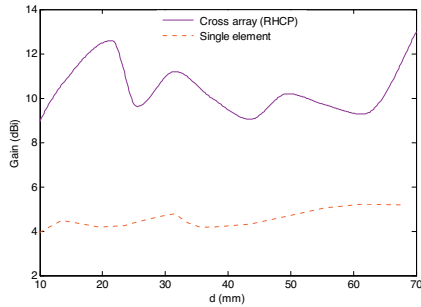


Figure 14. Gain against d at $f = 6.84$ GHz.

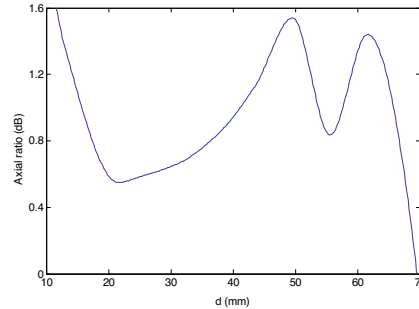


Figure 15. Axial ratio against d at $f = 6.84$ GHz.

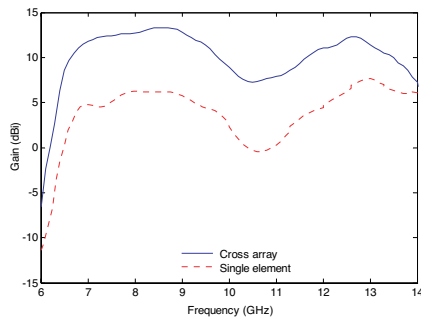


Figure 16. Frequency response of RHCP gain of the cross-shaped array.

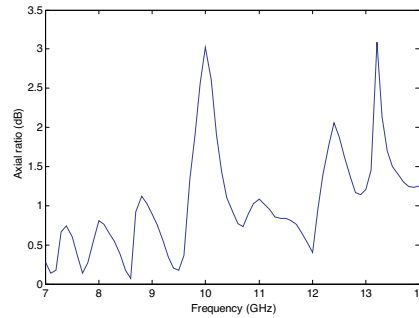


Figure 17. Frequency response of the axial ratio of the cross-shaped array.

4.2.3. Radiation Characteristics of the Square-Shaped Array

The square-shaped array, shown in Fig. 2(b) is excited with equal amplitudes and $+90^\circ$ progressive phase shift to obtain LHCP. Radiation patterns of the LHCP and RHCP components in the

elevation plane $\varphi = 90^\circ$ and in the cone $\theta = 15^\circ$ at different frequencies, are presented in Fig. 18.

Figure 19 shows the axial ratio of the square-shaped array at 7 GHz in the elevation plane at $\varphi = 90^\circ$ and on the cone $\theta = 15^\circ$. It is seen that the square-shaped array produces perfect LHCP in the forward directions determined by ($|\theta| < 28^\circ$) especially over narrow frequency bands around the cavity resonances.

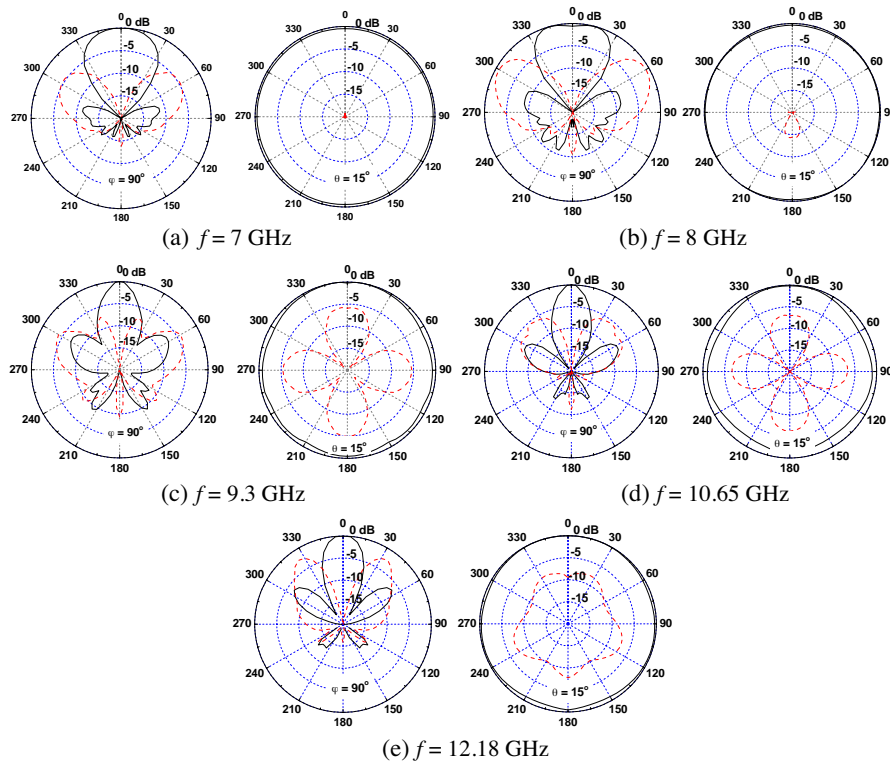


Figure 18. Radiation patterns for the circularly polarized components obtained for square-shaped array (solid line represents LHCP, dashed line represents RHCP).

The properties of square-shaped array patterns are summarized in Table 3. Good LHCP radiation characteristics are obtained from 7 GHz up to 9 GHz. The radiation pattern starts to deteriorate at 11 GHz. For the frequencies less than 11 GHz, the antenna has a beam width that ranges from 23° to 62° . The square-shaped array has a maximum gain of 13 dBi and maximum front to back ratio of 30 dB.

Figures 20 and 21 show the LHCP gain and the axial ratio against

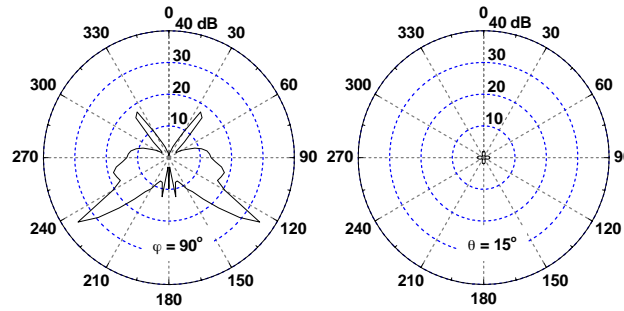


Figure 19. Axial ratio patterns for the square-shaped array at $f = 6.84$ GHz.

Table 3. Far field radiation properties for square-shaped array.

f (GHz)	3 dB BW	FBR (dB)	Gain (dBi)
7	56°	19.61	10.6
8	62°	26.2	6.73
9.3	24°	22.7	10.6
10.65	23.76°	26.7	13
12.18	27.8°	30.6	10.6

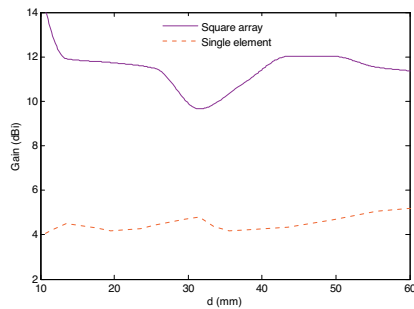


Figure 20. Gain against d at $f = 6.8$ GHz for the square-shaped array.

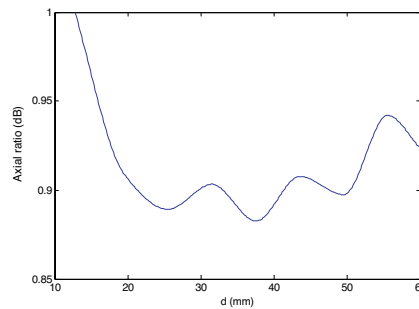


Figure 21. Axial ratio against d at $f = 6.8$ GHz for the square-shaped array.

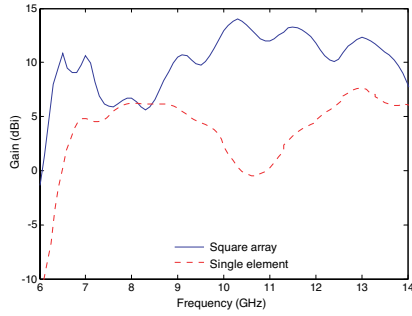


Figure 22. Frequency response of LHCP gain for the square-shaped array.

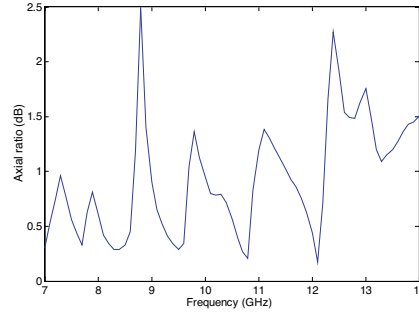


Figure 23. Frequency response of the axial ratio for the square-shaped array.

d. Figs. 22 and 23 show the frequency response of the LHCP gain and the axial ratio in the direction $\theta = 0^\circ$ and $\varphi = 90^\circ$ at $f = 6.84$ GHz, respectively. It can be observed that the LHCP gain of the square-array is ranged from 5.9 dBi to 14 dBi over the frequency band (9.5–12 GHz).

5. CONCLUSION

Cross-shaped and square-shaped arrays of CBS antennas are designed to produce circular polarization for X-band satellite communications. Good radiation characteristics of both arrays over some operating frequency bands have been observed. The proposed arrays can produce RHCP and LHCP with high gain and high front-to-back ratio, which is suitable for geostationary satellite-earth communications. The scattering parameters are studied over a wide frequency range where low return loss can be achieved (considering source impedances of 50 and 75) over the frequency bands of interest.

REFERENCES

1. Moheb, H., J. Shaker, and L. Shafai, "Numerical and experimental investigation of cavity-backed arbitrary antennas," *Can. J. Physics*, Vol. 74, No. 3–4, 122–131, 1996.
2. Hussein, K. F. A., "Effect of internal resonance on the radar cross section and shield effectiveness of open spherical enclosures," *Progress In Electromagnetics Research*, PIER 70, 225–246, 2007.
3. Jin, J. M. and J. L. Volakis, "A finite element-boundary integral formulation for scattering by three-dimensional cavity-backed

- apertures,” *IEEE Trans. Antennas & Propag.*, Vol. 39, No. 1, 97–104, Jan. 1991.
4. Omiya, M., T. Hikage, N. Ohno, K. Horiguchi, and K. Itoh, “Design of cavity-backed slot antennas using the finite-difference time-domain technique,” *IEEE Trans. Antennas Propagat.*, Vol. 46, 1853–1858, Dec. 1998.
 5. Hikage, T., M. Omiya, and K. Itoh, “Considerations on performance evaluation of cavity-backed slot antenna using the FDTD technique,” *IEEE Trans. Antennas Propag.*, Vol. 49, 1712–1717, Dec. 2001.
 6. Georgakopoulos, S. V., C. R. Birtcher, and C. A. Balanis, “Coupling modeling and reduction techniques of cavity-backed slot antennas: FDTD versus measurements,” *IEEE Trans. Antennas Propag.*, Vol. 43, 261–272, Aug. 2001.
 7. Shi, S., K. Hirasawa, and Z. Ning, “Circularly polarized rectangularly bent slot antennas backed by a rectangular cavity,” *IEEE Trans. Antennas Propag.*, Vol. 49, 1517–1524, Nov. 2001.
 8. Taflove, A., *Computational Electromagnetics*, Artech House, Norwood, MA, 1995.
 9. Luebbers, R. J. and H. S. Langdon, “A simple feed model that reduces time steps needed for FDTD antenna and microstrip calculations,” *IEEE Trans. Antennas Propagat.*, Vol. 44, 1000–1005, July 1996.
 10. Lubbers, R., K. Kunz, M. Schneider, and F. Hunsberger, “A finite difference time-domain near zone to far zone transformation,” *IEEE Trans. Antennas Propagat.*, Vol. 34, 429–433, Apr. 1991.
 11. Yee, K. S., “Numerical solution of initial boundary value problems involving Maxwell’s equations in isotropic media,” *IEEE Trans. Antennas and Propagation*, Vol. 14, 302–307, May 1966.
 12. Taflove, A. and S. C. Hagness, *Computational Electrodynamics: The Finite-Difference Time-Domain Method*, 3rd edition, Artech House, Norwood, MA, 2005.
 13. Taflove, A. and M. E. Brodwin, “Numerical solution of steady-state electromagnetic scattering problems using the time-dependent Maxwell’s equations,” *IEEE Trans. Microwave Theory Tech.*, Vol. 23, 623–630, Aug. 1975
 14. Tretyakov, O. A. and F. Erden, “Temporal cavity oscillations caused by a wide-band waveform,” *Progress In Electromagnetics Research B*, Vol. 6, 183–204, 2008.
 15. Kukharchik, P. D., V. M. Serdyuk, and J. A. Titovitsky, “Diffraction of hybrid modes in a cylindrical cavity resonator by a

- transverse circular slot with a plane anisotropic dielectric layer,” *Progress In Electromagnetics Research B*, Vol. 3, 73–94, 2008.
16. Hémon, R., P. Pouliguen, H. He, J. Saillard, and J.-F. Damiens, “Computation of EM field scattered by an open-ended cavity and by a cavity under radome using the iterative physical optics,” *Progress In Electromagnetics Research*, PIER 80, 77–105, 2008.
 17. Xu, L., J. Tian, and X.-W. Shi, “A closed-form solution to analyze RCS of cavity with rectangular cross section,” *Progress In Electromagnetics Research*, PIER 79, 195–208, 2008.
 18. Geyi, W., “Time-domain theory of metal cavity resonator,” *Progress In Electromagnetics Research*, PIER 78, 219–253, 2008.
 19. Wang, F. J. and J.-S. Zhang, “Wideband cavity-backed patch antenna for PCS/IMT2000/2.4 GHz WLAN,” *Progress In Electromagnetics Research*, PIER 74, 39–46, 2007.
 20. Mahajan, M., S. K. Khah, and T. Chakravarty, “Extended cavity model analysis of stacked circular disc,” *Progress In Electromagnetics Research*, PIER 65, 287–308, 2006.
 21. Bopp III, C. L. and C. M. Butler, “Analysis of transmission of a signal through a complex cylindrical/coaxial cavity by transmission line methods,” *Progress In Electromagnetics Research*, PIER 56, 33–51, 2006.
 22. Das, S., A. Chakrabarty, and A. Chakraborty, “Characteristics of an offset longitudinal/transverse slot coupled crossed waveguide junction using multiple cavity modeling technique considering the TE_{00} mode at the slot aperture,” *Progress In Electromagnetics Research*, PIER 67, 297–316, 2007.
 23. Wang, C.-F., Y. Xu, and Y.-B. Gan, “3-dimensional implementation of the field iterative method for cavity modeling,” *Progress In Electromagnetics Research*, PIER 47, 27–47, 2004.